ICAST2014 #066

Integrated Feedback/Feedforward Control of Flexible Spacecraft for Agile Attitude Maneuver and Vibration Suppression

Hiroshi Okubo[1], Shinya Kuwamoto[2]

[1] 1 Department of Mechanical Engineering, Kanagawa Institute of Technology, Atsugi, Japan
2 Graduate School of Engineering, Osaka Prefecture University, Sakai, Japan

Abstract

Because control moment gyroscopes (CMGs) are capable of generating a much larger control torque for attitude maneuvers than can reaction wheels (RWs), vibration becomes a significant issue for flexible structures such as solar paddles. This paper presents an integrated feedback/feedforward control system for reducing the vibration of flexible structures, as well as for completing a rapid, large-angle attitude maneuver of the spacecraft. The proposed Lyapunov control integrated with the Nil-Mode-Exciting (NME) profiler and an extended Input Shaping (IS) technique effectively improves the transient vibration of the modal response. The results of numerical simulations, based on the dynamics model of a typical flexible spacecraft, are shown for demonstrating the capability of the proposed control designs. In order to attenuate the residual vibration of the flexible structure more effectively, a new method is proposed for generating the feedforward input torque, i.e., the integrated NME profiler and Input Shaping. The integrated Lyapunov control using this input shaper is most effective in suppressing the transient vibration of the modal responses.

1. INTRODUCTION

In recent years, the attitude control of spacecraft using control moment gyros (CMGs) has attracted attention [1]-[3]. Because the CMGs are capable of generating a much larger control torque for attitude maneuvers than can reaction wheels (RWs), vibration becomes a significant issue for flexible structures such as solar paddles. It is important to address this issue for the agile attitude maneuver control of flexible spacecraft. This paper presents an integrated feedback/feedforward control for reducing the vibration of flexible structures, as well as for completing a rapid, large-angle attitude maneuver of the spacecraft. This paper describes the dynamics of flexible spacecraft and the principle of CMGs. Then, the feedback control based on Lyapunov stability theory is developed, in which the angular velocity, quaternion, and modal variables are used for feedback.

This paper then develops feedforward control based on Input Shaping (IS) and the Nil-Mode-Exciting profiler (NME). These methods are applied to the input commands to minimize the residual vibration and suppress the modal responses. The input shaping on the Posicast control proposed by Smith is one of the most effective vibration suppression techniques for a flexible structure [4]-[6]. The input shaping technique has been applied to the concurrent design with feedback control of nonlinear coupled vibration systems such

as trajectory tracking control of a flexible manipulator [7], and the slewing maneuver of a flexible spacecraft [8]. In this paper, we apply a method of input shaping to control the residual vibration by convoluting a sequence of impulses in a one-degree-of-freedom vibration system. One of the main advantages of input shaping is that the equation used to reduce the residual vibrations requires only estimates for the natural frequencies and damping ratios.

The NME profiler has been studied for shaping the input command to attenuate the vibration of the spacecraft appendage structures. It was applied to the hyper-precision attitude control of ASTRO-G [9], a Radio-Astronomical Satellite having a high-precision 9-meter deployment antenna. The input command is designed so as not to excite all modes of vibration; i.e., the generated command input has only frequency components lower than the lowest natural frequency of the flexible structure. The NME profiler is also employed in this paper for the suppression of residual vibrations due to the rest-to-rest maneuver of the spacecraft and it is integrated with the input shaping technique to achieve a superior performance in vibration damping.

2. DYNAMICS OF FLEXIBLE SPACECRAFTS WITH CMGS

The equations of motion of a flexible spacecraft with CMG can be described as follows;

$$\boldsymbol{J}\cdot\dot{\boldsymbol{\omega}}+\boldsymbol{Q}^{\boldsymbol{T}}\ddot{\boldsymbol{\eta}}+\boldsymbol{\omega}\times\left(\boldsymbol{J}\cdot\boldsymbol{\omega}+\boldsymbol{Q}^{\boldsymbol{T}}\dot{\boldsymbol{\eta}}\right)=\boldsymbol{\tau}+\boldsymbol{T}_{\boldsymbol{ext}} \tag{1}$$

$$\ddot{\boldsymbol{\eta}}+\boldsymbol{C}\dot{\boldsymbol{\eta}}+\boldsymbol{D}\boldsymbol{\eta}+\boldsymbol{Q}\dot{\boldsymbol{\omega}}=0 \tag{2}$$

$$\dot{\boldsymbol{h}}+\boldsymbol{\omega}\times\boldsymbol{h}=-\boldsymbol{\tau} \tag{3}$$

where the first equation describes the rotational motion of the spacecraft body where $\boldsymbol{J}$ is the inertia matrix of the satellite including CMGs; $\boldsymbol{\omega}=(\omega_1 \quad \omega_2 \quad \omega_3)^T$ is the spacecraft angular velocity vector; $\boldsymbol{\tau}=(\boldsymbol{\tau}_1 \ \boldsymbol{\tau}_2 \ \boldsymbol{\tau}_3)$ is the internal control torque generated by the CMGs; and $\boldsymbol{T}_{ext}$ is the external torque vector, which includes the gravity gradient, solar pressure, and aerodynamic torques. The second equation represents the dynamics of flexible structures by introducing the modal coordinate vector $\boldsymbol{\eta}(t)$; and $\boldsymbol{C}$, $\boldsymbol{D}$, and $\boldsymbol{Q}$ are the damping coefficient, natural frequency, and coupling matrices, respectively. Finally, the third equation describes the dynamics of the CMGs where $\boldsymbol{h}$ is the angular momentum vector of the CMGs expressed in the spacecraft body-fixed axes. These three equations are coupled with each other through the control torque and the inertial coupling terms in the equations.

In order to describe the attitude kinematics, we have the following quaternion kinematic differential equations as well. Details are described in the references, e.g., [1]-[3].

$$\begin{bmatrix}\dot{q}_0\\ \dot{q}_1\\ \dot{q}_2\\ \dot{q}_3\end{bmatrix}=\frac{1}{2}\begin{bmatrix}0 & \omega_3 & -\omega_2 & \omega_1\\ -\omega_3 & 0 & \omega_1 & \omega_2\\ \omega_2 & -\omega_1 & 0 & \omega_3\\ -\omega_1 & -\omega_2 & -\omega_3 & 0\end{bmatrix}\begin{bmatrix}q_0\\ q_1\\ q_2\\ q_3\end{bmatrix} \tag{4}$$

Since the angular momentum vector of the CMGs $\boldsymbol{h}$ is a function of gimbal angles $\boldsymbol{\delta}=(\delta_1,\ldots,\delta_n)^T$, the time derivative of the angular momentum is derived as

$$\dot{\boldsymbol{h}}=\boldsymbol{A}\dot{\boldsymbol{\delta}} \tag{5}$$

where $\mathbf{A} = \mathbf{A}(\delta)$ is the $3 \times n$ Jacobian matrix defined as

$$\boldsymbol{A} \equiv \frac{\partial \boldsymbol{h}}{\partial \boldsymbol{\delta}} = [\frac{\partial h_i}{\partial \delta_j}] \tag{6}$$

We consider a pyramid array of single-gimbal CMGs (SGCMGs) as shown in Fig. 1, where four SGCMGs are located on the faces of a pyramid, and the gimbal axes are orthogonal to the pyramid faces. In this case, each CMG has the same angular momentum and the skew angle is chosen as β=54.7° so that the momentum envelope becomes nearly spherical. The angular momentum vectors $\boldsymbol{h_i}$ are on the surface of the pyramid, and the angular momentum $\boldsymbol{h_i}$ is given as a function of $\boldsymbol{\delta_i}$ as follows

$$\boldsymbol{h} = \sum_{i=1}^{4} \boldsymbol{h}_i = \begin{bmatrix} -c\beta\, sin\, \delta_1 \\ cos\, \delta_1 \\ s\beta\, sin\, \delta_1 \end{bmatrix} + \begin{bmatrix} -cos\, \delta_2 \\ -c\beta\, sin\, \delta_2 \\ s\beta\, sin\, \delta_2 \end{bmatrix} \begin{bmatrix} c\beta\, sin\, \delta_3 \\ -cos\, \delta_3 \\ s\beta\, sin\, \delta_3 \end{bmatrix} + \begin{bmatrix} cos\, \delta_4 \\ c\beta\, sin\, \delta_4 \\ s\beta\, sin\, \delta_4 \end{bmatrix} \tag{7}$$

where, $c\beta = \cos\beta$ and $s\beta = \sin\beta$, and the Jacobian matrix $\boldsymbol{A}$ is given by

$$\boldsymbol{A} = \begin{bmatrix} -c\beta cos\, \delta_1 & sin\, \delta_2 & c\beta cos\, \delta_3 & -sin\, \delta_4 \\ -sin\, \delta_1 & -c\beta cos\, \delta_2 & sin\, \delta_3 & c\beta cos\, \delta_4 \\ s\beta cos\, \delta_1 & s\beta cos\, \delta_2 & s\beta cos\, \delta_3 & s\beta\, cos\, \delta_4 \end{bmatrix} \tag{8}$$

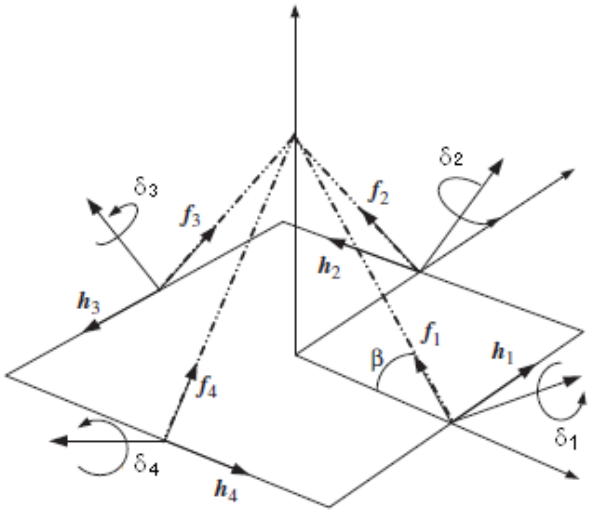

Figure 1. Cluster of four SGCMGs in pyramid configuration

.

From (3) and (5), the spacecraft torque input $\boldsymbol{u}$ is given by

$$\dot{\boldsymbol{h}} \equiv \boldsymbol{u} = -\boldsymbol{\tau} - \boldsymbol{\omega} \times \boldsymbol{h} \tag{9}$$

$$\boldsymbol{u} = \boldsymbol{A}\dot{\boldsymbol{\delta}} \tag{10}$$

and the gimbal angular rate vector can be obtained with the pseudoinverse of $\boldsymbol{A}$:

$$\dot{\boldsymbol{\delta}} = \boldsymbol{A}^{+}\boldsymbol{u} \tag{11}$$

where $\boldsymbol{A}^{+} = \boldsymbol{A}^{T}(\boldsymbol{A}\boldsymbol{A}^{T})^{-1}$.

This steering law is called the Moore-Penrose steering logic and provides the gimbal angular rate for generating a desired input torque. However, there is a singular point problem that is peculiar to CMGs. Avoidance of the singular condition is requisite for agile, large-angle maneuvers of a flexible spacecraft. A singularity robust steering algorithm is applied to avoid this problem. One of these is shown in the literature [Wie, B. 2000], which introduces artificial terms in the diagonal elements to avoid the singularity of matrix inversion.

$$\mathbf{A}^{+} = \mathbf{A}^{T}\left(\mathbf{A}\mathbf{A}^{T} + \kappa\mathbf{I}\right)^{-1} \tag{12}$$

3. FEEDBACK CONTROL DESIGN

We derive a feedback control law for the pointing control of flexible spacecraft, as well as vibration suppression of flexible appendage structures.

By introducing the attitude quaternion vector $\begin{bmatrix} q_0 \\ q_1 \\ q_2 \\ q_3 \end{bmatrix} = \begin{bmatrix} q_0 \\ \boldsymbol{q} \end{bmatrix}$, a positive Lyapunov function is proposed as

$$\boldsymbol{V} = \left[(q_0 - 1)^{\mathbf{2}} + \boldsymbol{q}^{\boldsymbol{T}}\boldsymbol{K}_{\boldsymbol{P}}\boldsymbol{q}\right] + \frac{1}{2}\boldsymbol{\omega}^{T}\boldsymbol{J}_{\boldsymbol{mb}} \cdot \boldsymbol{\omega} + \frac{1}{2}[\boldsymbol{\eta}^{\boldsymbol{T}},\ \boldsymbol{\psi}^{\boldsymbol{T}}]\boldsymbol{P}_{1}\begin{bmatrix}\boldsymbol{\eta} \\ \boldsymbol{\psi}\end{bmatrix} \tag{13}$$

where $\boldsymbol{J}_{\boldsymbol{mb}} = \boldsymbol{J} - \boldsymbol{Q}^{T}\boldsymbol{Q} \geq 0$, $\boldsymbol{\psi}$ is the inertial velocity of flexible structures, $\boldsymbol{\psi} = \dot{\boldsymbol{\eta}} + \boldsymbol{Q}\boldsymbol{\omega}$, $\boldsymbol{K}_{P} = \kappa\boldsymbol{I} \geq 0$ and $\boldsymbol{P}_{1} = \boldsymbol{P}_{1}^{T} \geq 0$. The time derivative of the Lyapunov function is derived as

$$\begin{aligned}\dot{\boldsymbol{V}} &= \boldsymbol{\omega}^{T}[\boldsymbol{K}_{\boldsymbol{P}}\boldsymbol{q} - \boldsymbol{\omega} \times (\boldsymbol{J}_{\boldsymbol{mb}} \cdot \boldsymbol{\omega} + \boldsymbol{Q}^{T}\boldsymbol{\psi}) + \boldsymbol{Q}^{\boldsymbol{T}}(\boldsymbol{C}\boldsymbol{\psi} + \boldsymbol{D}\boldsymbol{\eta} - \boldsymbol{C}\boldsymbol{Q}\boldsymbol{\omega}) + \boldsymbol{\tau}] \\ &\quad + [\boldsymbol{\eta}^{\boldsymbol{T}},\ \boldsymbol{\psi}^{\boldsymbol{T}}]\boldsymbol{P}_{\mathbf{1}}\left[\begin{bmatrix}\mathbf{0} & \boldsymbol{I} \\ -\boldsymbol{D} & -\boldsymbol{C}\end{bmatrix}\begin{bmatrix}\boldsymbol{\eta} \\ \boldsymbol{\psi}\end{bmatrix} - \begin{bmatrix}\boldsymbol{I} \\ -\boldsymbol{C}\end{bmatrix}\boldsymbol{Q}\boldsymbol{\omega}\right]\end{aligned} \tag{14}$$

If we use the control torque satisfying the following condition

$$\boldsymbol{\tau} = -\boldsymbol{F}\begin{bmatrix}\boldsymbol{q} \\ \boldsymbol{\eta} \\ \boldsymbol{\psi}\end{bmatrix} - \boldsymbol{K}_{\boldsymbol{d}}\boldsymbol{\omega} \tag{22}$$

where

$$\boldsymbol{F} = \left[\boldsymbol{K}_{\boldsymbol{P}},\ \boldsymbol{Q}^{\boldsymbol{T}}\left[\begin{bmatrix}\boldsymbol{D} \\ \boldsymbol{C}\end{bmatrix} - \boldsymbol{P}_{\mathbf{1}}\begin{bmatrix}\boldsymbol{I} \\ -\boldsymbol{C}\end{bmatrix}\right]^{\boldsymbol{T}}\right],\ \boldsymbol{K}_{\boldsymbol{d}} = \boldsymbol{K}_{\boldsymbol{d}}^{\boldsymbol{T}} \geq 0 \tag{15}$$

the time derivative of the Lyapunov function is negative definite.

$$\dot{\boldsymbol{V}} = -\boldsymbol{\omega}^{\boldsymbol{T}}\left(\boldsymbol{K}_{\boldsymbol{d}} + \boldsymbol{Q}^{\boldsymbol{T}}\boldsymbol{C}\boldsymbol{Q}\right)\boldsymbol{\omega} - [\boldsymbol{\eta}^{\boldsymbol{T}},\ \boldsymbol{\psi}^{\boldsymbol{T}}]\boldsymbol{P}_{\mathbf{1}}\begin{bmatrix}\boldsymbol{\eta} \\ \boldsymbol{\psi}\end{bmatrix} \leq \mathbf{0}$$

Where the matrix $\boldsymbol{P}_{\mathbf{1}}$ is derived from a matrix Lyapunov equation as follows:

$$\boldsymbol{P_1}\begin{bmatrix}\boldsymbol{0} & \boldsymbol{I}\\ \boldsymbol{-D} & \boldsymbol{-C}\end{bmatrix}-\begin{bmatrix}\boldsymbol{0} & \boldsymbol{I}\\ \boldsymbol{-D} & \boldsymbol{-C}\end{bmatrix}^{\boldsymbol{T}}\boldsymbol{P_1}=\boldsymbol{-2R_1} \tag{16}$$

and $\boldsymbol{P_1}=\boldsymbol{P_1^T}>0,\ \boldsymbol{R_1}=\boldsymbol{R_1^T}>0.$

The block diagram of the feedback control is illustrated in Fig. 2. By using the Lyapunov control law and designing the gains $\boldsymbol{K_d}$ and $\boldsymbol{F}$ appropriately, we can converge the state vector $x=[q^T,\eta^T,\psi^T,\omega^T\ ]^T$ to the demanded state quickly:

$$\boldsymbol{\tau_d}=\boldsymbol{-F}\begin{bmatrix}\boldsymbol{q_d-q}\\ \boldsymbol{\eta_d-\eta}\\ \boldsymbol{\psi_d-\psi}\end{bmatrix}-\boldsymbol{K_d}(\boldsymbol{\omega_d-\omega}) \tag{17}$$

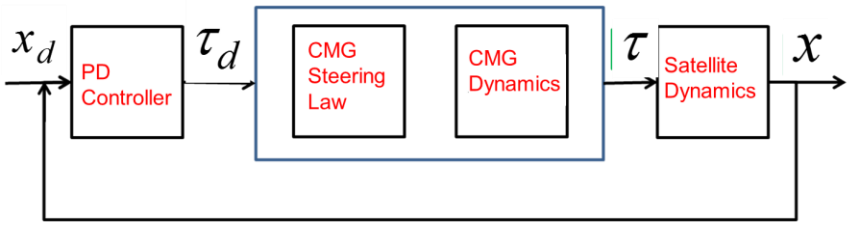

Figure 2. Block diagram of Feedback controller

4. FEEDFORWARD CONTROL DESIGN

4.1 Input shaping technique for vibration suppression

The amplitude of the vibration response when N impulses are fed to the one-degree-of-freedom vibration system is given as follows:

$$A_{amp}=\sqrt{\left(\sum_{j=1}^{N}B_j\,cos\,\omega_d t_j\right)^2+\left(\sum_{j=1}^{N}B_j\,sin\,\omega_d t_j\right)^2} \tag{18}$$

Where

$$B_j=A_j\frac{\omega_0}{\sqrt{1-\zeta^2}}exp\left(-\zeta\omega_o\left(t_N-t_j\right)\right) \tag{19}$$

In addition, A_j denotes the amplitude of the jth impulse; t_j, the time at which the impulses occur; ω0, the natural frequency of the system; and ζ, the damping ratio of the system. To eliminate the vibrational response after the input has been applied, the expression for A_{amp} should be zero at time t_N, then the input ends. That is, both of the squared terms in (18) should be independently equal to zero.

$$\sum_{j=1}^{N}A_j\,exp\left(-\zeta\omega_o\left(t_N-t_j\right)\right)cos\,\omega_d t_j=0 \tag{20}$$

$$\sum_{j=1}^{N}A_j\,exp\left(-\zeta\omega_o\left(t_N-t_j\right)\right)sin\,\omega_d t_j=0 \tag{21}$$

For example, consider two impulse inputs at times t_1 and t_2 with amplitudes A_1 and A_2. The responses to the two impulse inputs cancel each other, and the vibrations after time t_2 vanish only if the natural frequency and damping ratio of the system are known exactly. For the successful application of the input shaping in most real systems, the constraint equations, i.e., (20) and (21), must ensure robustness to modeling errors. Singer and Seering [6] have developed a method of robust input shaping by using the condition that the derivative of (20) and (21) with respect to the frequency of the residual vibration equals zero. The resulting shaper is called a zero vibration and derivative (ZVD) shaper. Please refer to their study for details.

Figure 3 shows an example of ZVD shaping. The single unit step input is divided into the sequence of three inputs with smaller amplitudes and time sift satisfying the "input shaping" conditions.

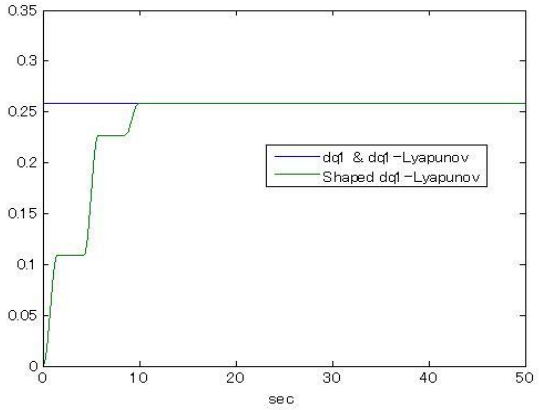

Figure 3. Input shaping for a step command

4.2 Nil-Mode-Exciting profiler

The concept of Nil-Mode-Exciting profiler is based on the use of the sinc function

$$sinc(t) = \frac{\sin(\omega_0 t)}{\omega_0 t} \tag{22}$$

A Fourier transform of the sinc function shows the characteristics of an ideal low-pass filter with a cutoff frequency of ω_0 rad⁄s. The frequency response function and time history of the sinc function are shown in Fig. 4.

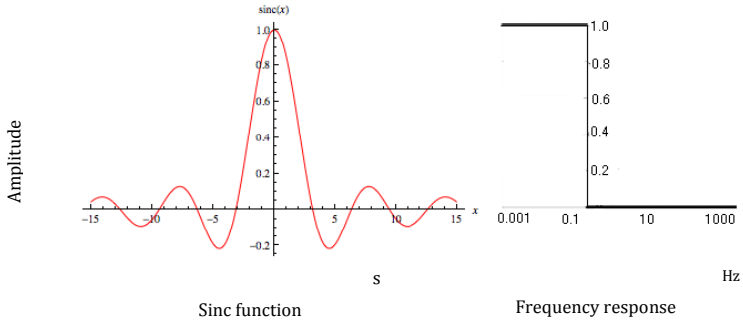

Figure 4. Characteristics of a sinc function

An NME profiler consists of a couple of sinc functions with opposite signs as follows:

$$A = \frac{\sin\{\omega_a(t-t_{offset1})\}}{\omega_a(t-t_{offset1})} - \frac{\sin\{\omega_a(t-t_{offset2})\}}{\omega_a(t-t_{offset2})} \tag{23}$$

where

$$t_{offset2} - t_{offset1} = \frac{2\pi}{\omega_a} \tag{24}$$

Equation (23) represents the sum of the accelerating and decelerating functions with time offsets. A typical synthesized sinc function is shown in Fig. 5.

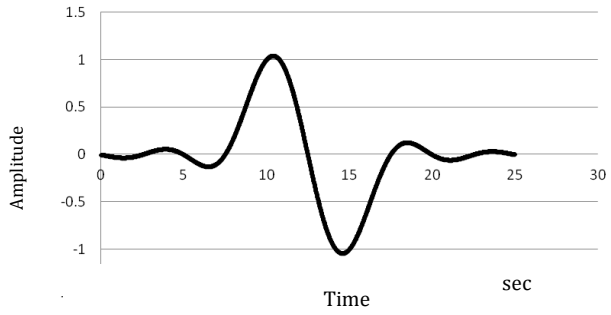

Figure 5. A synthesized sinc function for NME

Practically, to modify the above infinite sinc function into a finite-time function, it is necessary to introduce a time window function such as a Hamming function:

$$w(x) = 0.54 - 0.46\cos 2\pi x \quad (\text{if } 0 \le x \le 1) \tag{25}$$

4.3 Integration of Input Shaping and Nil-Mode-Exciting profiler

The third method is newly developed in this paper. In Fig. 6, a single NME profile for the torque input (red line) is divided into three inputs (dotted lines) according to the sequence of three inputs for the Input Shaping (Fig. 3).

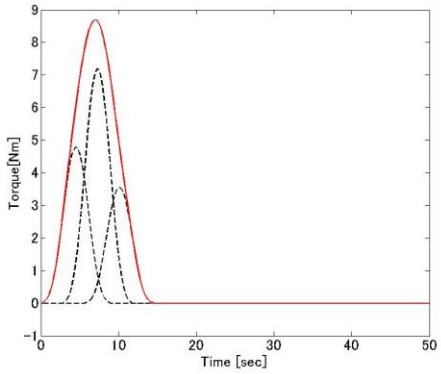

Figure 6. Integrated Input Shaping and NME profiler

5. NUMERICAL SIMULATIONS

The proposed feedback and feedforward control designs can be demonstrated using the dynamic model of a flexible spacecraft. The configuration and mass parameters of the spacecraft and the dynamics model of the flexible structure shown in the literature were used for the numerical simulation [13]. The results of the numerical simulation are briefly summarized for this dynamics model. The initial and final conditions of the simulation are listed in Table 2; these correspond to a 180° rotation of the spacecraft around the x-axis.

Figures 7-10 demonstrate the effectiveness of using the singularity avoidance control ([11], [12]), for a large-angle, agile maneuver. Figures 7 and 8 are the time histories of the quaternion and the first-mode modal displacement, respectively, without singularity avoidance. Figures 9 and 10 show the improved responses obtained with the singularity avoidance control. However, the vibration response in Fig. 10 is still excessive at the initial and final stages of the spacecraft maneuver, due to the high magnitude of the control torque generated by the CMGs.

$$J = \begin{bmatrix} 1543.9 & -2.3 & -2.8 \\ -2.3 & 471.6 & -35 \\ -2.8 & -35 & 1713.3 \end{bmatrix} \ [\mathrm{kgm}^2] \qquad Q = \begin{bmatrix} -9.4733 & -15.5877 & 0.0052 \\ -0.5331 & -0.4855 & 18.0140 \\ 0.5519 & 4.5503 & 16.9974 \\ -12.1530 & 11.7138 & -0.0002 \\ -0.0289 & 0.0199 & 6.2378 \\ 0.2268 & 0.8289 & -35.7298 \\ -0.8935 & 5.4516 & 1.5005 \\ 1.1628 & 2.6350 & -0.0989 \\ -0.1688 & 0.3131 & 3.6231 \\ -1.4910 & 2.0020 & -0.2893 \end{bmatrix} [\mathrm{kgm}]$$

Table 1. Natural frequencies and damping coefficients

Mode No.	Nat. Freq.	Damping
1st	0.7400	0.004
2nd	0.7500	0.005
3rd	0.7600	0.0064
4th	0.7600	0.0080
5 th	1.1600	0.0085
6 th	3.8500	0.0092

Table 2. Initial and target state values

Initial value	ω_0	$[0 \quad 0 \quad 0]^T \quad rad/\sec$
	q_0	$[1 \ 0 \ 0 \ 0]$
	δ_0	$[0 \ 0 \ 0 \ 0] \quad rad$
	$\dot{\delta}_0$	$[0 \ 0 \ 0 \ 0] \quad rad/sec$
	η_0	$[0]$
	$\dot{\eta}_0$	$[0]$
	ψ_0	$[0]$
	$\dot{\psi}_0$	$[0]$
Target values	ω_f	$[0 \quad 0 \quad 0]^T \quad rad/\sec$
	q_f	$[0 \ 1 \ 0 \ 0]$

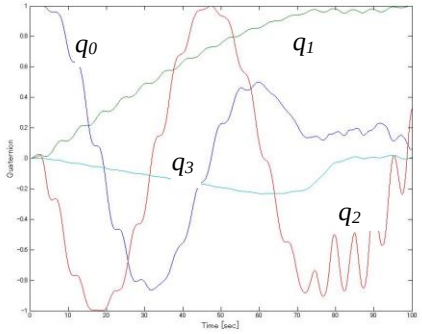

Figure 7. Quaternion (without singularity avoidance)

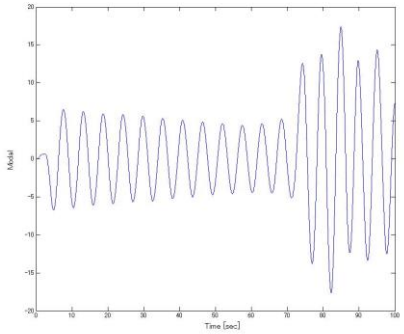

Figure 8. First mode response (without singularity)

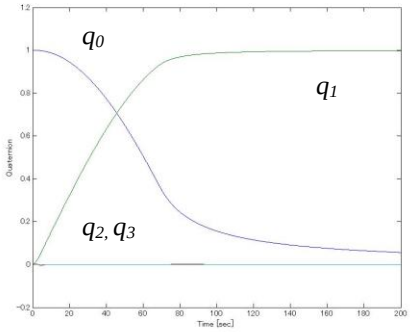

Figure 9. Quaternion (with singularity avoidance).

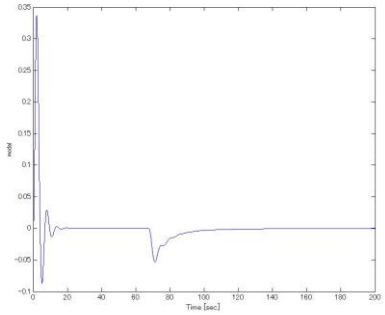

Figure 10. First mode response (with singularity avoidance).

To attenuate the residual vibration of the flexible structure, three different methods were examined for generating the input torque:

1) Lyapunov control with Input Shaping,
2) Lyapunov control with NME profiler, and
3) Lyapunov control with integrated NME profiler and Input Shaping.

The feasibility of the first method was demonstrated in our previous research [10]. This method can suppress the residual vibration of the flexible structure to some extent. However, the result is less effective than the second method, and it is therefore not shown in this paper.

The effectiveness of the Nil-Mode-Exciting profiler is shown in Figs. 11 and 12. The magnitude of the first-mode structural vibration is suppressed compared with the results without NME. However, a vibration of small amplitude remains during and after the maneuver.

The result of the advanced feedback/feedforward control is summarized in Figs. 13 and 14. The numerical simulations show that the integrated NME profiler and Input Shaping approach is promising for suppressing the vibration of the flexible structures in a large-angle, rapid maneuver.

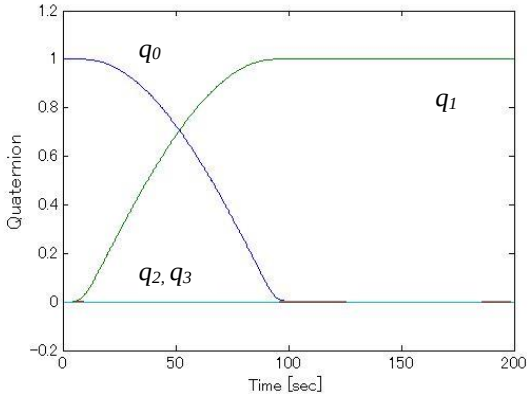

Figure 11. Quaternion (with NME profiler).

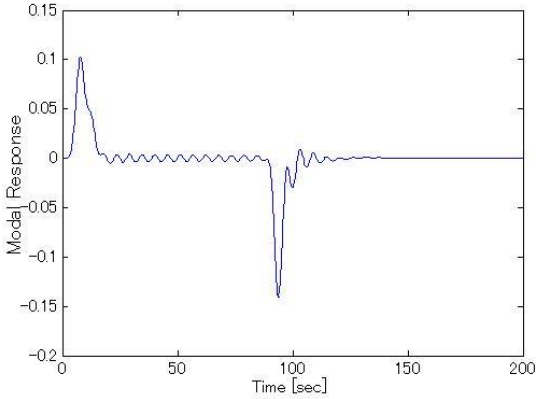

Figure 12. First mode response (with NME profiler).

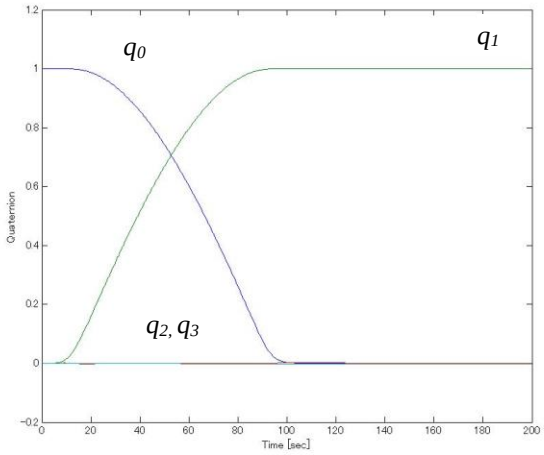

Figure 13. Quaternion (with Integrated NME/IS).

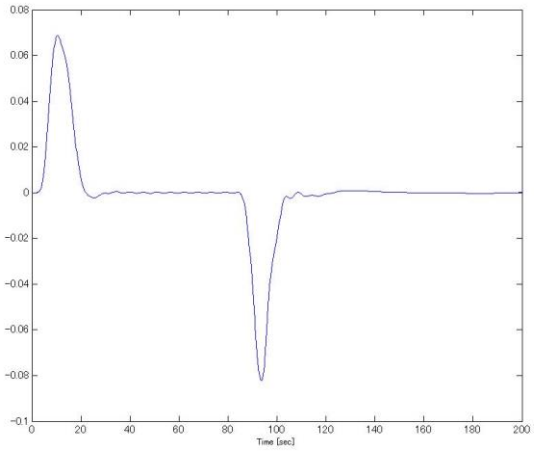

Figure 14. First mode response (with Integrated NME/IS)

6. CONCLUSION

In this paper, integrated control laws using Lyapunov stability theory with an NME profiler and/or Input Shaping have been proposed for CMG-controlled agile attitude maneuvers of flexible spacecraft. The Lyapunov control with the NME profiler or Input Shaping is effective both in the attitude control and in the residual vibration reduction of the flexible structure. Furthermore, the integrated Lyapunov control using the NME profiler and Input Shaping effectively improves the transient vibration of the modal response.

REFERENCES

1. Kwon, S. and Okubo, H., "Angular Velocity Stabilization of Spacecraft Using Two Single-Gimbal Control Moment Gyros", Proc. of the 26th International Symposium on Space Technology and Science, 2008-d-16, 2008, 6 pages.
2. Kwon, S., Okubo, H., and Shimomura, T., "Pointing Control of Spacecraft Using Two Single-Gimbal Control Moment Gyros", Trans. JSASS, Aerospace Tech. Japan, Vol. 8, No. ists27, 2012, pp. Pd_105-Pd_111.
3. Kwon, S., Tani, Y., Okubo H., and Shimomura, T., "Fixed-Star Tracking Attitude Control of Spacecraft Using Single-Gimbal Control Moment Gyros", American Journal of Engineering and Applied Sciences, Vol. 3, No. 1, 2010, pp. 865– 871.
4. Smith, O.J.M., Feedback Control Systems, McGraw-Hill, New York, 1958, p.338.
5. Singhose, W.E., "Extra-Insensitive Input Shaper for Controlling Flexible Spacecraft", Journal of Guidance, Control and Dynamics, Vol. 19, No. 2, 1996, pp. 385–391.
6. Singhose, W.E., Banerjee, A.K., and Seering, W.P., "Slewing Flexible Spacecraft with Detection-Limiting Input Shaping", Journal of Guidance, Control and Dynamics, Vol. 20, No. 2, 1997, pp. 291–298.
7. Hasegawa, Y. and Okubo, H., "Input Shaping for Fast Trajectory racking Control of a Flexible Manipulator", Proceedings of the MOVIC, Paper 327, 10 pages, 2008.
8. Kashima, M., "Attitude Control of Flexible Spacecraft Using Control Momentum Gyros", Master Thesis, Graduate School of Engineering, Osaka Prefecture University, February 2010.
9. Kamiya, T., Maeda, K., Ogura, N., Hashimoto, T., and Sakai, S., "Preshaping Profiler for Flexible Spacecraft Rest-to-Rest Maneuvers", JAXA-ISAS, 229-8510, Japan.
10. Kim, J.-J. and Agrawal, B.N., "Rest-To-Rest Slew Maneuver of Three-Axis Rotational Flexible Spacecraft", Proceedings of The 17th World Congress of the International Federation of Automatic Control, Seoul, Korea, July 6–11, 2008.
11. Kurokawa, H., "A Geometric Study of Single Gimbal Control Moment Gyros – Singularity Problems and Steering Law-", Mechanical Engineering Laboratory Report, No. 140, 1987.
12. Okubo, H. and Tani, Y., "Singularity Robust Steering of Redundant Single Gimbal Control Moment Gyros for Small Satellites", Proc. of the 8th International Symposium on Artificial Intelligence, Robotics and Automation in Space, Munich, Germany, 2005, pp. 1–8.
13. Likins, P. W., Marsh, E. L., and Fleischer, G. E., "Flexible Spacecraft Control System Design Procedures Utilizing Hybrid Coordinates", NASA/JPL Technical Memorandum 33-493, September 15, 1971.